Combined Theoretical Modeling of Photoexcitation Spectrum of an Isolated Protonated Tyrosine

Jang Sook Kwon, Chang Min Choi, Hwan Jin Kim, and Nam Joon Kim*

Department of Chemistry, Chungbuk National University, Cheongju, Chungbuk 361-763, South Korea

Joonkyung Jang

Department of Nanomaterials Engineering, Pusan National University, Miryang 627-706, South Korea

Mino Yang*

Department of Chemistry and Basic Sciences Research Institute, Chungbuk National University, Cheongju, Chungbuk 361-763, South Korea

Received: October 29, 2008; Revised Manuscript Received: January 2, 2009

A photodepletion spectrum of gaseous protonated tyrosine molecules was obtained at 150 K by a UV laser spectroscopic technique in conjunction with mass spectrometry and interpreted by theoretical methods. The spectrum exhibits three distinct bands separated each other by about 800 cm^{-1}. Stable conformers of the molecular ion were determined by quantum mechanical density functional theory, and their electronic transition energies were obtained by a semiempirical quantum chemistry calculation. The whole pattern of the spectrum was reasonably reproduced by a combination of theoretical methods, the second-order cumulant expansion, a semiempirical quantum chemistry method, molecular dynamics simulation, and a semiclassical time-correlation function approach. The three spectral bands turned out to arise from the vibronic transition of two vibrational modes constituted by the "benzene breathing" mode and a torsional mode of the amino acid backbone. It is suggested that the major factor in spectral broadening is not conformational disorder or lifetime broadening but thermal fluctuation of the stable conformers. The good agreement between experimental and theoretical spectra exemplifies the validity of the theoretical methods applied for the present molecular system.

I. Introduction

Three natural aromatic amino acids, phenylalanine (Phe), tyrosine (Tyr), and tryptophan (Trp), absorb ultraviolet radiation strongly. These amino acids have been the subject of many theoretical and experimental studies because they are mainly responsible for photochemistry and photophysics of proteins in the near-UV region and are employed as probes for studying molecular interactions in proteins.

Studies of the biomolecules in vivo environments are complicated by the intrinsic properties of the molecules and the roles of solvents or nearby proteins. Therefore, it is desirable to examine the former factor in the absence of the latter. Experimental techniques to investigate biomolecules isolated from the solvent environment were limited by the nonvolatility of such molecules, which makes it difficult to prepare samples in the gas phase. Despite this difficulty, Levy and co-workers[1] developed a technique to generate a supersonic molecular beam of neutral Trp molecules, and spectroscopic techniques began to emerge as one of the useful tools to study the molecular properties of isolated biomolecules.

Levy and co-workers[2] utilized the supersonic molecular beam technique to obtain the electronic spectrum of Trp in the gas phase; they found that several stable conformers of Trp can exist and the complex behavior of the molecules in solution could be studied by analyzing the molecular properties in the gas phase. Using the same technique, Martinez et al.[3] studied the conformational dependence of electronic excitation energy of Tyr in the gas phase and found that phenol ring vibrational modes are the major contribution to the vibronic bands appearing in its fluorescence emission spectrum. The vibronic spectra of Trp and Tyr were obtained with a very high spectral resolution by Lindinger et al.,[4] who used helium droplets to lead the temperature extremely low and partially confirmed the conformational assignments of the bands made by Levy and co-workers. In the helium droplets environment, the number of distinct absorption bands was reduced and the authors suggested a few plausible origins of the spectral differences. Grace et al.[5] analyzed the vibronic transition bands of Tyr in terms of the vibrational modes studied by IR and Raman spectra and quantum chemical calculation. Complete conformational analysis of a gaseous Tyr molecule was recently carried out by Zhang et al.[6] using various levels of quantum chemical calculations. They concluded that conformations of the molecule are stabilized by intramolecular hydrogen bonding between the carboxylic and amino groups and further by additional interaction between the amino group and π-electrons of the phenol ring.

Recently, in addition to the studies performed on the neutral forms of biological molecules, experimental techniques to study the charged organic and biological molecules were developed by a few groups with a combination of mass spectrometry and laser spectroscopy.[7–9] Such experimental techniques seem to be very useful in revealing the intrinsic properties of the biological molecules in charged forms often occurring naturally in biological systems. As a demonstration of the method, Boyarkin et al.[9] compared the temperature-dependent photof-

* Corresponding authors: e-mail namjkim@chungbuk.ac.kr (N.J.K.) or MinoYang@chungbuk.ac.kr (M.Y.).

10.1021/jp809573a CCC: $40.75
Published on Web 02/26/2009

ragmentation spectra of protonated tryptophan ($TrpH^+$) and tyrosine ($TyrH^+$) and found that the excited electronic state of $TrpH^+$ decays very rapidly on a time scale shorter than 100 fs. The rapid decay of excited $TrpH^+$ is believed to arise from internal conversion induced by the coupling of a localized $\pi\pi^*$ state with a dissociative $\pi\sigma^*$ state.[10]

In contrast with $TrpH^+$, the excited electronic state of $TyrH^+$ was found to be substantially stable and its spectrum at an ambient temperature was thought to be thermally broadened without any electronic decay processes. Similar behavior was observed in a pump−probe photofragment study performed by Kang et al.,[8] and those authors attributed the difference in the decay time scales of the two protonated amino acids to a difference in the coupling strength between the $\pi\pi^*$ and $\pi\sigma^*$ states. High-level quantum calculations using a coupled-cluster method have been performed to reveal the properties of the excited electronic states of $TrpH^+$ and $TyrH^+$ by Grégoire et al.,[11] and they found that the dissociative $\pi\sigma^*$ state is really in the vicinity of the optically excited $\pi\pi^*$ state with an energy gap larger in $TyrH^+$ than in $TrpH^+$.

Apart from such valuable findings from the temperature-dependent study via gas-phase spectroscopy, the photofragmentation spectrum of $TyrH^+$ measured at an ambient temperature exhibited two bands centered, respectively, at 35 300 and 36 100 cm^{-1}, where the band appearing at the higher energy is larger in intensity.[9] The multiple bands may originate from (1) vibronic transition, (2) photofragmentation yield varying with the excitation energy, (3) existence of the higher singlet electronic state, and (4) conformational disorder. In order to understand the photochemistry of $TyrH^+$, it is important to reveal the mechanisms of the appearance of multiple bands and spectral broadening. That is our goal in the experimental aspect pursued in the present paper. For this, we performed photodissociation spectroscopy in combination with mass spectrometry for the gaseous molecular ion at a moderately low temperature (150 K).

An appropriate theoretical modeling method is required to extract molecular dynamic information from the experimental results. Rigorous methods for theoretical modeling are quite complicated and computationally too expensive to be applied for the study of complex biomolecules because one needs a fully quantum mechanical description of molecular dynamics. A usual approach to overcome the complication is to employ the second-order cumulant expansion technique, which has been shown to be useful for the study of molecular dynamics in the condensed phase by various types of linear or nonlinear optical spectroscopy.[12,13] Since the second-order cumulant expansion technique was developed with some restrictions, its validity is not always guaranteed.[14] The key quantity needed in the approach is the equilibrium time correlation function of transition energy. With a few exceptions,[15−17] the time correlation functions are often modeled by simple expressions such as Gaussian, exponential, and trigonometric functions with adjustable parameters.[13,18] By comparing experimental results with the theoretical response functions that are the functionals of the time correlation function, one may obtain the information of molecular dynamics represented by a set of adjustable parameters.

A more sophisticated approach is to nonempirically calculate the time correlation function through a combination of various levels of theory, for example, classical molecular dynamics simulation, quantum chemistry calculation, and a semiclassical method to consider the effect of quantum nuclear dynamics. Due to many uncertainties implicit in each method, the accuracy of calculations in concert with theoretical methods still should be tested by comparing their predictions with experimental

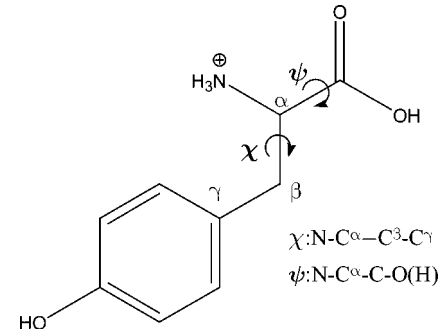

Figure 1. Molecular structure of $TyrH^+$.

results. Recently, Gorbunov et al.[17] discussed the validities of various aspects of the theories applied in the calculation of condensed-phase vibrational spectra and concluded that a quantitative first-principle prediction of IR absorption spectra is limited. While the theoretical approaches above have been widely used for condensed-phase electronic or vibrational spectroscopies, as far as we know, those have never been applied in the spectral analysis of gas-phase spectroscopy. In this paper, we successfully applied those approaches, for the first time, in predicting the shape of our gas-phase photodepletion spectrum.

The molecular structure of $TyrH^+$, along with the definitions of two dihedral angles specifying the molecular conformation, is shown in Figure 1. The protonation site is assumed to be the amino group. Assuming that the excitation-energy dependence of the photodepletion yield should result mainly from the energy dependence of molecular absorption probability, we calculate the electronic transition energies of a few low-lying conformers of $TyrH^+$. We also perform the molecular dynamics simulation and a series of quantum chemical calculations for fluctuating conformations of the molecular ion. With those results, a quantum-mechanical time correlation function of the electronic transition energy is approximately calculated by virtue of a semiclassical approach utilizing a quantum correction factor. The quantum correction factor takes into account the quantum effects of nuclear motion in the time correlation function obtained from the classical MD simulation. The time correlation function generates a theoretical absorption spectrum, which is compared with the experimental photodepletion spectrum. From the comparison, the mechanisms of the spectral broadening and appearance of the multiple bands are explained in terms of conformational disorder and fluctuation/relaxation dynamics of nuclear motion. Four major results obtained in our work are summarized as follows.

(1) Absorption spectra of four stable conformers of $TyrH^+$ are theoretically calculated and compared with experimental photodepletion spectrum

(2) The multiple bands observed in the experiment turned out to be caused by vibronic transition of the symmetric breathing mode of phenol ring coupled to the torsional mode of the amino acid backbone.

(3) Present theories support the spectral broadening mechanism of each band to be thermal broadening.

(4) We established the validity of the employed theoretical approaches, at least, when they are applied to linear spectra of the relatively large molecule in the gas phase.

II. Experimental and Theoretical Methods

A. Experimental Method. The experimental apparatus (Figure 2) is a quadrupole ion-trap reflectron time-of-flight mass spectrometer (QIT-reTOFMS). Since the details were described

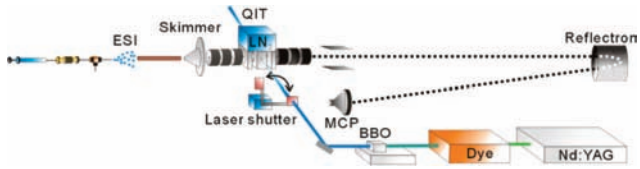

Figure 2. Experimental setup: ESI-QIT-reTOF mass spectrometer.

elsewhere,[19] only a brief description is given here. The powder sample of tyrosine was dissolved in a solvent mixture of methanol, water, and acetic acid (48.5:48.5:3 by volume) at a concentration of 100 μM. The solution was electrosprayed into droplets through a nozzle floated to +3.5 kV and introduced into the vacuum through a metal capillary heated up to 80 °C for desolvation. The resulting ions were transferred to a QIT through a skimmer with a hole of 0.38-mm diameter.

QIT consists of one ring and two endcap electrodes. Each endcap has a hole of 3-mm diameter for ion beams to enter and exit and the ring electrode has four holes of 2.2-mm diameter, two of which were used for laser beams to enter and exit. With both endcaps grounded, a radio frequency (rf) signal of a constant frequency (1 MHz) and amplitude (+2.5 kV) was applied to the ring electrode to accumulate ions. A coldfinger of a liquid nitrogen (LN_2) reservoir was attached to the QIT to lower the temperature. For more efficient cooling of the ions, helium was introduced into the ion trap via a metal tube that went through the LN_2 reservoir. QIT was also enclosed with a heat shield. With all of these, the temperature of QIT fell down to 150 ± 5 K. We regarded that the temperature of $TyrH^+$ is same with that of the QIT, with the assumption that fast thermal equilibrium between the trapped ions and the QIT is achieved through multiple collisions with helium buffer gas inside the QIT.[20]

After 48 ms of ion accumulation, an electrical pulse was applied to the skimmer to prevent the entrance of subsequent ions to the QIT. Then, the broadband stored waveform inverse Fourier transform (SWIFT)[21] waveforms were applied to the exit endcap for isolation of $TyrH^+$ from other residual ions in the QIT. The SWIFT waveforms were generated by an arbitrary function generator (AFG 3022, Tektronix) using the algorithm developed by Doroshenko and Cotter.[22]

Following repetitive application of the SWIFT waveform for 50 ms, the frequency-doubled output (~2 mJ/pulse) of a dye laser (ScanMate II, line width 0.15 cm^{-1}) pumped by the second harmonic of an Nd:YAG laser was irradiated into the QIT to induce photodissociation of the isolated ions. Coumarin 540A dye was used to cover the wavelength region of this study. Then a positive DC pulse was applied to the entrance endcap to extract all of the parent and photofragment ions into a reflectron TOF-MS for mass analysis. Photofragment ions at m/z 119, 123, 136, and 147 were detected. During this extraction, the rf voltage in the ring electrode was turned off. The ions traveled the field-free drift region, reverted by the reflectron, and were detected by a microchannel plate (MCP). The ion signals from MCP were processed by a digital storage oscilloscope. The timings of the trapping, laser firing, and ion extraction were all synchronized by TTL pulses from a digital delay generator.

The electronic absorption probability was obtained by recording photodepletion of $TyrH^+$ at m/z 182 as a function of the laser wavelength. The photodepletion yield (I_{pd}, percent) was determined by

$$I_{pd} = \frac{I_{off} - I_{on}}{I_{off}} \times 100 \quad (1)$$

where I_{on} and I_{off} are the intensities of parent ions with and without laser pulses, respectively. They were measured by turns at each wavelength, as we blocked and unblocked the laser pulses using a laser shutter. From the measurement of the power dependence of the laser pulse, the photodepletion of $TyrH^+$ is found to be a single-photon process. We observed a slope of ~0.7 in the plot of log (I_{pd}) versus log (laser power).

B. Theoretical Method. On the supposition that the photodepletion yield is proportional to the frequency-dependent absorption probability,[23] we introduce the theoretical methods employed in this work to calculate the absorption spectrum of the molecular ion. First, the dependence of electronic structure on the conformational variation is examined. We performed molecular dynamics (MD) simulations to search for stable conformations of the molecules. The temperatures of the simulations were set high enough (600 K) for the molecules to surmount the conformational activation barrier. For the MD simulation we used the Gromacs package[24] with the OPLS-AA force field.[25] The searched conformations were reoptimized by density functional theory (DFT; level B3LYP/6-31G) and the resulting geometries were again used as initial structures for further optimization at a higher level of theory (B3LYP/6-311++G**). Single-point energies and vertical (S0−S1) transition energies of the final conformations were calculated, respectively, by B3LYP/6-311++G** and by the semiempirical method[26] (ZINDO/S) implemented in the Gaussian 03 package.[27] In addition to those single-point calculations, we also performed the equilibrium MD simulation at 150 K and a series of the quantum chemical computations based on ZINDO/S to theoretically reproduce the shape of the absorption spectrum.

It is well-known[28] that perturbation theory gives the frequency-dependent absorption coefficient, $\alpha(\omega)$, responsible for the spectral shape as the Fourier transform of the time correlation function of dipole moment:

$$\alpha(\omega) \sim \omega(1 - e^{-\beta\hbar\omega})I(\omega) \quad (2)$$

where β is the Boltzmann factor and

$$I(\omega) = \int_{-\infty}^{\infty} dt\, e^{i\omega t}\langle\mu(t)\mu\rangle_{eq} \quad (3)$$

is called the line shape function, which is proportional to the transition probability induced by the absorption of a single photon of frequency ω. Here μ and $\mu(t)$ are, respectively, the dipole operator of a chromophore molecule in the direction of electric field of irradiated light and its time evolution, $\mu(t) = e^{iHt/\hbar}\mu e^{-iHt/\hbar}$, with the molecular Hamiltonian H. The broken bracket notation $\langle\rangle_{eq}$ in eq 3 denotes the ensemble average over the equilibrium density matrix. To evaluate the average, one should take a trace over the electronic and nuclear quantum states.

Since the excited electronic state of $TyrH^+$ is known to live very long (>22.3 ps),[9,11] the lifetime broadening contributes little to the absorption spectrum and the molecular ion can be, within the time scale of our interest, safely assumed to be of a electronic two-state system signified by g and e. In this case, the molecular Hamiltonian and the dipole operator are written, respectively, as $H = \sum_{i=g,e} |i\rangle H_i \langle i|$ and $\mu = \sum_{i,j=g,e} |i\rangle \mu_{ij} \langle j|$. Since only the ground electronic state is assumed to be populated in equilib-

rium, the time correlation function of dipole operator is constituted by two terms: the autocorrelation functions of permanent (μ_{gg}) and transition (μ_{eg}) dipoles. The former is negligible in eq 3 due to nonresonant condition in the integral, and only the latter survives.

If we employ the Condon approximation for the transition dipole (μ_{eg} is assumed to be constant), eq 3 is further approximated as

$$I(\omega) = |\mu_{eg}|^2 \int_{-\infty}^{\infty} \mathrm{d}t\, \mathrm{e}^{i\omega t} \left\langle \exp\left(\frac{iH_g t}{\hbar}\right) \exp\left(-\frac{iH_e t}{\hbar}\right) \right\rangle_{\mathrm{eq}} \quad (4)$$

The validity of the Condon approximation for the present molecular system is discussed in section III. Equation 4 is the time-domain expression of the Franck−Condon absorption spectrum and is given by the Fourier transform of the time-dependent overlap between the nuclear wave function in the ground electronic state and the wavepacket evolving in the excited electronic state. The formula tells us that the nuclear fluctuations in the ground electronic state and the relaxation of wavepacket in the excited electronic state determine the absorption line shape of the system. Of course there would be additional lifetime broadening if the excited electronic state decayed rapidly via a certain mechanism, which is not the case for $TyrH^+$ discussed above.

Since H_g and H_e in eq 4 are quantum-mechanical operators in the nuclear space, it is not easy to enumerate the line shape function. Therefore in order to make the calculations amenable, one expands the product of the two propagators in eq 4 with respect to its cumulants and truncates it at the second order.[29] In this approach, the line shape function (eq 4) is simplified to

$$I(\omega) = |\mu_{eg}|^2 \int_{-\infty}^{\infty} \mathrm{d}t \exp[i(\omega - \omega_{eg})t - \int_0^t \mathrm{d}t_1 \int_0^{t_1} \mathrm{d}t_2\, C(t_2)] \quad (5)$$

where ω_{eg} is the average of the vertical transition frequencies when the chromophore molecules are in thermal equilibrium in the ground electronic state. $C(t)$ in eq 5, which is the key quantity carrying all the microscopic information necessary for calculating the line shape, is the time correlation function describing static and dynamic fluctuations of the electronic transition energy:

$$C(t) \equiv \frac{1}{\hbar^2} \langle \delta E(t) \delta E \rangle_{\mathrm{eq}} \quad (6)$$

where $\delta E \equiv (H_e - H_g) - \langle H_e - H_g \rangle_{\mathrm{eq}}$.

We note that the time evolution of the transition energy in eq 6, $\delta E(t) = \mathrm{e}^{iH_g t/\hbar} \delta E \mathrm{e}^{-iH_g t/\hbar}$, is governed by the nuclear dynamics occurring in the *ground* electronic state. Namely, both of the nuclear fluctuations and relaxation dynamics determining the line shape are described by the fluctuation dynamics in the ground electronic state simply via the time correlation function (eq 6). In principle, if all orders in the cumulant expansion of eq 4 were given, the former could be exactly described by the latter with more complicated time correlation functions. Although truncation of the cumulant expansion at the second order is exact only for the Gaussian statistics of transition energy, its usefulness may be extended to more general cases with the capability of predicting the fundamental features of spectral broadening induced by nondissociative nuclear dynamics occurring in the two electronic states. Therefore, within the framework of the second-order cumulant expansion, the nuclear dynamics in the two electronic states is represented, hereafter, by the fluctuation dynamics in the ground electronic state.

We note that if the nuclear motions coupled to the electronic transition are modeled as independent harmonic modes whose equilibrium positions in each electronic state are displaced from each other, the statistics of transition energy is Gaussian and the second-order cumulant approximation becomes exact.[29] Of course, if the potential surface of the excited electronic state is greatly different from that of the ground electronic state, the present approach may break down in quantitative predictions of line shape. As we will show later, however, the present theoretical approach is successful in reproducing the experimental spectrum and it is one of the important conclusions derived in this work to illustrate the usefulness of the employed theories for describing the absorption spectrum of the present molecular system.

Although nuclear quantum effects must be considered for the accurate evaluation of $C(t)$, it is highly demanding to perform a fully quantum-mechanical computation for obtaining the time evolution of such a complex molecule. If the nuclear motion of molecule is classical, however, it is much easier to calculate the time correlation function. Therefore, we performed the molecular dynamics simulation at the experimental temperature to mimic the nuclear fluctuations in the ground electronic state. Following the trajectory in the conformational space, a series of quantum chemical calculations were done to calculate the time-dependent energy gap $H_e - H_g$. The time correlation function calculated in this way is denoted by $C_{\mathrm{cl}}(t)$, where the subscript cl signifies classical nuclear dynamics.

Of course, the quantum characteristics of nuclear motion cannot be properly described by classical mechanics. However, many theoretical efforts to find a way of incorporating nuclear quantum effects into such a classical time correlation function have been reported.[30−34] In this paper we will employ a semiclassical approximation in which the time correlation function for a *classical* molecule is corrected by a certain factor called quantum correction factor Q. More specifically, the Fourier transform of the quantum correlation function $\tilde{C}(\omega)$ is approximately obtained from that of the classical correlation function $\tilde{C}_{\mathrm{cl}}(\omega)$ by use of the relationship $\tilde{C}(\omega) = \tilde{C}_{\mathrm{cl}}(\omega)\tilde{Q}(\omega)$. By doing this, the effects of quantum nuclear dynamics are approximately introduced in our calculation and an asymmetric shape of the line shape function (which is the case often observed in experiments but is not realized from the cumulant expansion model for classical nuclear dynamics) may be obtained. A few forms of the quantum correction factor have been suggested by several authors.[32,35] Berne and Harp[30] and Oxtoby[31] suggested one so-called "standard" approximation: $\tilde{Q}(\omega) = 2/(1 + \mathrm{e}^{-\beta\hbar\omega})$, and we will employ the approach in this paper.

We first generate a nuclear trajectory by performing the molecular dynamics simulation for a single $TyrH^+$ at 150 K. The Berendsen temperature coupling method[36] with a temperature coupling time constant of 0.1 ps was used for the isothermal condition. The time dependence of the electronic transition energy was obtained from a series of semiempirical ZINDO/S calculations with 6000 conformations of the molecule generated by the molecular dynamics simulation.

Here we discuss more details about how the absorption spectrum is related to the quantum time correlation function and what physical processes are described by eq 5. Due to the complex propagator in quantum mechanics, the quantum time

correlation function is divided into real and imaginary parts, $C(t) = C'(t) + iC''(t)$, and similarly its Fourier transform is written as a sum of two terms, $\tilde{C}(\omega) = \tilde{C}'(\omega) + \tilde{C}''(\omega)$. We note that these two terms are real and satisfy the symmetry relations $\tilde{C}'(-\omega) = \tilde{C}'(\omega)$ and $\tilde{C}''(-\omega) = -\tilde{C}''(\omega)$ as a result of the time-reversal symmetry, $C(-t) = C^*(t)$, in the time domain. We note that the approximate quantum time correlation function constructed above with the quantum correction factor satisfies the symmetry relations. If we replace the time correlation function in eq 5 with its Fourier transform and use the symmetry relations, the line shape function is rewritten in terms of three terms, each of which corresponds to a distinct vibronic transition process:

$$I(\omega) = |\mu_{eg}|^2 \int_{-\infty}^{\infty} \mathrm{d}t\, e^{i(\omega-\omega_{eg}^0)t} \exp[-\int_0^{\infty} d\omega'\, J(\omega')(2\bar{n}_{\omega'} + 1)] \times \exp[\int_0^{\infty} d\omega'\, J(\omega')e^{-i\omega' t}] \exp[2\int_0^{\infty} \mathrm{d}\omega'\, J(\omega')\bar{n}_{\omega'} \cos(\omega' t)] \quad (7)$$

where $\omega_{eg}^0 \equiv \omega_{eq} - \lambda$ is the purely electronic transition energy and

$$\lambda \equiv \int_0^{\infty} \mathrm{d}\omega\, \omega J(\omega) \quad (8)$$

is the reorganization energy associated with the S0−S1 transition.

$$J(\omega) \equiv \frac{\tilde{C}''(\omega)}{\pi\omega^2} \quad (9)$$

is the spectral density, which corresponds to the vibrational density of states weighted by their vibronic coupling strengths. $\bar{n}_{\omega} \equiv (e^{\beta\hbar\omega} - 1)^{-1}$ is the thermal occupation number of the mode of a frequency ω. For harmonic nuclear motions linearly coupled to electrons, the spectral density is independent of temperature[29] and the temperature dependence of the line shape results only from $\bar{n}_{\omega}$ in eq 7.

Equation 7 includes three exponential terms depending on the spectral density. The first is, so-called, the Debye−Waller factor, which has nothing to do with the shape of spectrum but influences the temperature dependence of the total absorption intensity. The second and third exponential terms are responsible for the vibronic transitions, respectively, from the ground and excited (hot) vibrational states of vibrational modes. Equation 7 tells us that the line shape is determined by the convolution of the spectra associated with the two processes. In the notes above, we tried to show that eq 5 written in time domain captures the usual frequency-domain picture of absorption processes.

III. Results and Discussion

Using the experimental technique described in section II, we measured the photodepletion yield (I_{pd}) of $TyrH^+$ at 150 K. The maximum of the yield was about 40% at 35 215 cm^{-1}. We calibrated the raw data in order to remove an artifact arising from nonuniformity in the power of excitation laser over the frequency. Then the calibrated data may be comparable to the absorption line shape function of the molecular ion. The calibrated photodepletion yield as a function of the excitation energy in wavenumber is displayed in Figure 3. Three bands in the spectrum are apparent. The spectrum was fitted by three Gaussian functions as displayed in the figure and they are centered, respectively, at 35 310, 36 100, and 36 960 cm^{-1}. The

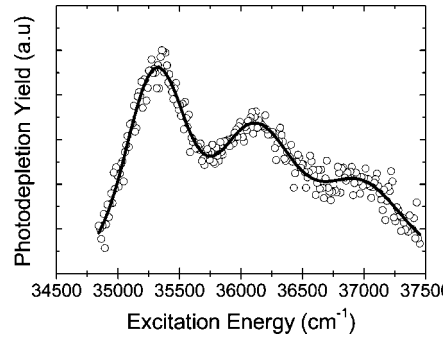

Figure 3. Experimental photodepletion spectrum of $TyrH^+$ measured at 150 K. The solid curve shows fitting of the data with three Gaussian functions centered, respectively, at 35 215, 36 006, and 36 862 cm^{-1}.

three bands are split from each other with an energy gap of about 800 cm^{-1}. The lowest-energy band is broadened about full width at half-maximum (fwhm) = 470 cm^{-1}, while the second and third bands are a bit broader (fwhm ~ 640 cm^{-1}). The energies of the two lower bands are almost the same as those measured at ambient temperature by Boyarkin et al.,[9] but on the contrary, the relative intensities of the two peaks were reversed. As the temperature of the sample was cooled down to 150 K in this work, the intensity of the second band became weaker than that of the first band.

First, we examine the dependence of the electronic transition energy of $TyrH^+$ on the conformational inhomogeneity. Analyzing the MD trajectory carried out at 600 K, we selected 20 conformations of $TyrH^+$ with a low potential energy. They are reoptimized by the DFT methods as described in section II and reduced to eight different conformers with lowest energies. Figure 4 shows Newman projection diagrams of four of them along with their energies. In all four conformers, the hydrogen atom of the hydroxyl group on the phenol lies in the plane of the phenol ring, trans to the NH_3^+ group. The other four, which are not shown here, are the conformational isomers in which the rotation angle of the hydroxyl group is reversed and, hereafter, are indicated by a prime on the conformer letters. They are almost isoenergetic with their counterparts (A′ and B′ have been calculated to be higher in energy, respectively, by 0.1 and 0.5 kJ/mol[37] than A and B). The four conformers shown in Figure 4 are characterized by the two dihedral angles χ and ψ defined in Figure 1. For convenience later, the IUPAC definition of a dihedral angle varying from −180° through 180° is adopted for χ, while ψ is defined in a way that its values vary from 0° through 360°.

The values for conformer A, which is predicted to be the most stable one, are $\chi = -52°$ and $\psi = 169°$, where the NH_3^+ group lies above the phenol ring in an eclipsed form and the carboxylic group is pointing away from the phenol ring. This conformer seems to be stabilized by hydrogen-bond interactions of the NH_3^+ group with π electrons on the phenol ring and oxygen of the C═O group.

The dihedral angles of conformer B, which is 2.8 kJ/mol higher in energy than conformer A, are $\chi = 47°$ and $\psi = 186°$. In this conformer, both NH_3^+ and carboxylic groups lie above the phenol ring. Conformers A and B differ from each other mainly by a $2\pi/3$ rotation of the amino acid moiety along the dihedral angle χ. The potential barrier for isomerization between the two conformers was found to be about 15 kJ/mol in our DFT calculations (not presented), and therefore it is believed that the conformers do not easily transform to each other at the low temperature (150 K).

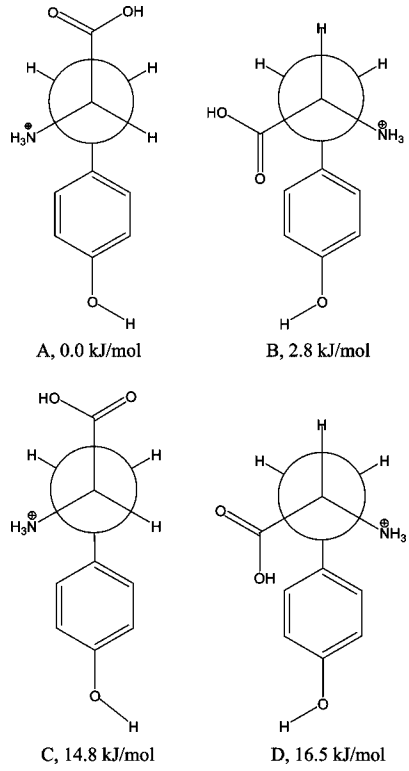

Figure 4. Newman projection diagrams of the four conformers of $TyrH^+$ that were found to be locally stable in the B3LYP/6-311++G** calculation. Relative electronic energy corrected by zero-point energy is shown for each diagram.

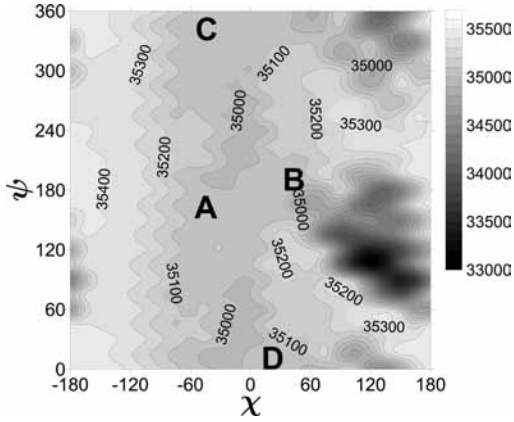

Figure 5. Two-dimensional map for the S0−S1 transition energy (in reciprocal centimeters) as a function of the dihedral angles χ and ψ calculated by the ZINDO/S method. The bar diagram on the right indicates the scale of the transition energy in reciprocal centimeters.

Conformers A and B (including A′ and B′) were also suggested to be the most stable ones with an energy gap of 2.7 kJ/mol in the study of Stearns et al.[37] Based on the comparison of infrared spectra and frequencies obtained from B3LYP/6-31++G** calculation, these authors concluded that conformer A is the global minimum conformation. We note that, in contrast to the B3LYP method, conformer B was more stable than conformer A by about 3 kJ/mol in the study using the MP2 calculation.[11]

Figure 5 shows two-dimensional contour plots of the S0−S1 transition energies as a function of the two dihedral angles χ and ψ while the other conformational variables are adiabatically optimized. The calculated transition energies vary from 35 000 to 35 400 cm^{-1} for the whole range of the angles except about $\chi = 120°$, where the carboxylic group faces the phenol ring plane. Transition energies for the latter domain were predicted to be lower by about 1500 cm^{-1} than the other domain, and therefore interaction of the carboxylic group with the phenol ring seems to make the transition energy red-shifted. However, since the conformations with $\chi \sim 120°$ are much higher in potential energy, they are unlikely to contribute to the spectrum. We note that although the calculated transition energies for the plausible conformations are coincident with the energy of the lowest band in the experimental spectrum, a quantitative comparison of the transition energy with the experimental result should not be made until the effects of vibronic transition are clarified as below. The S2 state was calculated to be much higher in energy, by about 5000 cm^{-1}, than the S1 state, and thus we exclude the possibility that the multiple bands observed in the photodepletion spectrum arise from excitation to the S2 state.

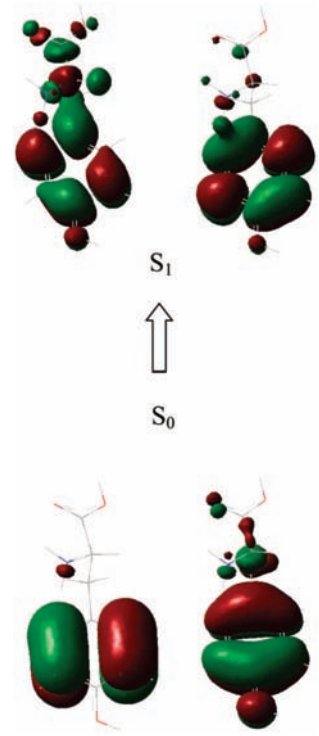

Figure 6. Most relevant molecular orbitals involved in the S0−S1 transition of conformer A of $TyrH^+$. The molecular orbitals of conformer B are similar in shape.

Although it has been discussed that non-Condon effects in vibrational spectroscopy can be large for strongly hydrogen-bonded systems,[38] the oscillator strength associated with electronic transition of the present system was calculated to be more or less insensitive to the conformational fluctuations around the stable conformers (not presented). This validates the Condon approximation [see eq 5] we employed in calculating the spectrum of the present molecular system.

S0−S1 transition energies for the stable conformers A and B were calculated to be 35 090 and 34 970 cm^{-1}, respectively. The S1 state of $TyrH^+$ is mainly constituted by the $\pi\pi^*$ transition of the phenol ring as depicted in the molecular orbital representation (calculated by ZINDO/S) of Figure 6. The $\pi\pi^*$ transition energy of an isolated phenol was calculated to be 36 460 cm^{-1} by the same method as above, and therefore, hydrogen bonding of the phenol ring with the NH_3^+ group seems to make the transition energy of the phenol ring redder.

The four stable conformers A, A′, B, and B′ were predicted to be different in transition energies only by a maximum of 120 cm^{-1}. Therefore, conformational inhomogeneity should not

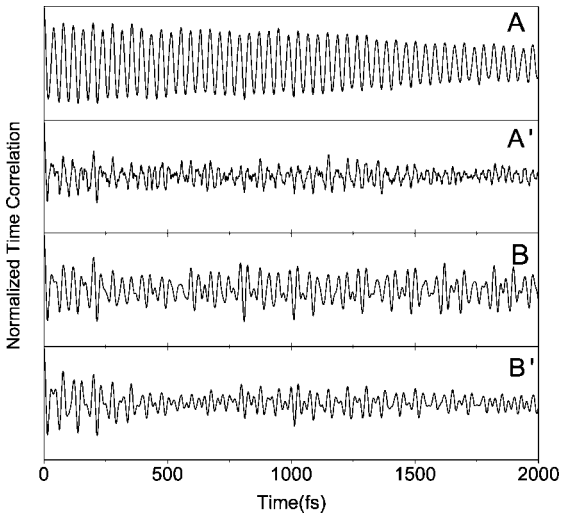

Figure 7. Time correlation functions of the four conformers normalized by their initial values.

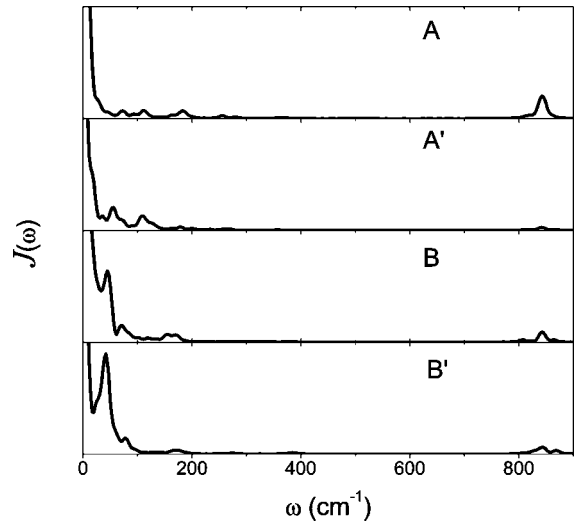

Figure 8. Spectral densities of the four conformers in arbitrary units. No vibronically active modes are out of the frequency range in the figure.

be the major source of the line broadening observed in the experiment. This is further supported by the fact that, with the higher energy of conformer B over A, the relative population of B at the electronic ground state will be very small, resulting in little contribution of B in the spectrum. As discussed in the Introduction, the S1 state of $TyrH^+$ is believed to be long-lived compared with the inverse bandwidth of the vibronic bands, and in this case, the major contribution to the line broadening may simply come from the nuclear fluctuation/relaxation in the ground and excited electronic states of the two stable conformers. To simulate such an effect, we employ the theoretical methods discussed in section II.

We carried out separate molecular dynamics simulations for conformers A, A′, B, and B′ in equilibrium at 150 K. During the whole simulation time (100 ps), isomerization among the conformers did not occur. However, conformer A remained stable only for 20 ps and then changed to conformer C, which is calculated to be higher in energy (see Figure 4) by DFT calculations. The instability of A shown in the simulation is a result of the force field, which predicts the energy of C to be lower than that of A. For each conformer, a part of the trajectory with a time period of 6 ps was selected with an arbitrary initial point and the time-dependent electronic transition energies of the selected conformations were calculated. With these fluctuating transition energies, in Figure 7, we evaluated the classical time correlation functions of the transition energy, $C_{cl}(t)$, which is the starting quantity in the calculation of the line shape function.

In the figure, one can see a distinct oscillation with a period of about 40 fs, which should be caused by large vibronic couplings of the oscillators classically vibrating with the period in the ground electronic state. Upon manipulation with the quantum correction factor, the oscillatory behavior gives rise to multiple vibronic bands with the corresponding frequency ($\sim$800 cm^{-1}) in the absorption spectrum. Therefore we suggest that the three experimental bands with splitting energies about 800 cm^{-1} should be the vibronic bands associated with the oscillation in Figure 7. The appearance of the oscillation with such a high frequency in the correlation function of transition energy implies the necessity of a quantum description such as the quantum correction factor. It takes about 4 ps for the amplitude of time correlation function to decay up to 10% of initial value. Therefore, we introduced an exponential decay function with a time constant of 1 ps into the correlation function upon its numerical Fourier transform for numerical stability. The addition of this function introduces artificial broadening by a few wavenumbers, which is negligible compared to the experimental absorption width.

In order to examine the spectral density responsible for the line shape (see eq 9), we take the Fourier transform of the classical time correlation function, $\tilde{C}_{cl}(\omega)$. The quantum time correlation function is constructed by the method described in section IIB as $\tilde{C}(\omega) = 2\tilde{C}_{cl}(\omega)/(1 + e^{-\beta\hbar\omega})$. Using the symmetry relations of the quantum time correlation function, $\tilde{C}''(\omega) = [\tilde{C}(\omega) - \tilde{C}(-\omega)]/2$, we obtain the spectral density, $J(\omega)$, defined in eq 9, and the result is presented in Figure 8. The spectral density distribution appears to be sensitive to conformational change; even reversal of the OH rotation angle on the phenol ring leads to a variation in the spectral density (compare A with A′ and B with B′). Besides the large amplitude at the frequency around $\sim$840 cm^{-1}, which is responsible for the prominent oscillation in Figure 7, one can see a wide distribution of spectral density over frequencies below 200 cm^{-1}, which is comparable to the thermal energy at 150 K. In particular, the modes with frequencies less than 50 cm^{-1} appear to be very strongly coupled to the electronic transition. Those modes should be thermally excited at 150 K and cause the thermal broadening of line shape. Therefore we suggest that the thermal motion of the low-frequency vibrational modes (<200 cm^{-1}) should be the spectral broadening mechanism of the individual vibronic bands observed in our experiment.

One may argue whether such low-frequency modes exist in the isolated small molecule. Vibrational progressions with frequencies of 42 and 52 cm^{-1} have been experimentally resolved in the photofragmentation spectrum of $TyrH^+$ measured at 6 K.[37] Normal mode analysis has been performed under the force field we used, and we found that five modes indeed have frequencies lower than 100 cm^{-1}. Also, frequency calculation by a quantum chemistry method (B3LYP/6-31+G*) predicts three normal modes below that frequency. We note, however, that since the spectral density includes nonlinear vibronic coupling terms as well as linear terms, the modes found in spectral analysis of the time correlation function should not necessarily be exactly matched to the normal modes probed by vibrational spectroscopies or analyzed by force fields or quantum chemistry calculations; though they might be well correlated.

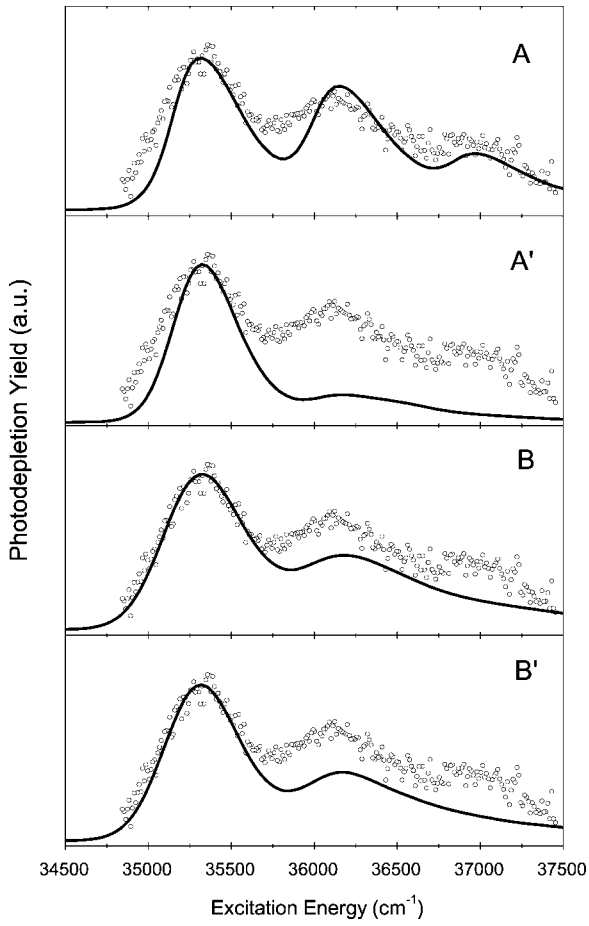

Figure 9. Experimental depletion yield and theoretical line shape functions. Vertical transition energies of the theoretical calculations were shifted to match the theoretical and experimental peak maxima.

We calculated the line shape functions and they were predicted to be dependent on molecular conformation, as expected from the distinct distributions of spectral density in Figure 8. Figure 9 shows line shapes for the four conformers in comparison with the experimental spectrum. Vertical transition energies of the conformers were shifted in order to match locations of peak maxima to those of the experimental spectrum. A well-defined structure of three bands was predicted by theory only for conformer A while it is barely seen for A′ since the amplitude of the spectral density at 840 cm^{-1} is the most prominent in conformer A but negligible in A′ (Figure 8). The vibronic structure in conformers B and B′ is weaker than in A and also than in the experiment. Meanwhile, the widths of the 0−0 transition band in B and B′ are a little wider than in A and A′ and in better agreement with experimental data. Enhanced spectral density at the frequencies of 40∼50 cm^{-1}, as displayed in Figure 8, is responsible for the wider 0−0 transition band in B and B′. In the aspect of vibronic bands, conformer A better represents the experimental spectrum, while in the aspect of thermal broadening width, conformers B and B′ do better. Therefore it is hard to conclude which conformer is the dominant component in our experiment. The experimental spectrum could be quantitatively compared with a proper superposition of those individual spectra if accurate information on vertical transition energies and relative populations of the four conformers were known. Even though the DFT calculation predicts that conformers B and B′ could not be thermally populated at 150 K, it is noted that those conformers have been experimentally identified even at much lower temperature (6 K).[37]

The reasonable agreement between line shape functions and experimental spectrum supports our claims for the mechanisms of the appearance of three bands and the spectral broadening of each band. The theory, however, does a worse job in *quantitative* prediction of the side bands. The discrepancy may be ascribed to frequency-dependent photofragmentation rate, anharmonicity of the excited electronic state, or simply to accuracy of the ZINDO/S method.

The splitting energy of the vibronic bands in the line shape function is about 840 cm^{-1}, which is a little larger than that in the experimental spectrum (about 800 cm^{-1}). The validity of the current theory lies in the assumption that the frequency of each mode in the ground electronic state should remain invariant in the excited electronic state. In reality, however, the frequency in the excited electronic state is usually lower than in the ground electronic state. This may be a reason for the discrepancy in the splitting energies of the spectral bands in the experimental spectrum (measuring the excited-state frequency) and the line shape function (reflecting the ground-state frequency). There is also a possibility that the force field may not be sufficiently accurate for the isolated molecular system.

The main feature of the S1 state of $TyrH^+$ arises from the phenol ring as illustrated in Figure 6. Therefore, one may expect that the vibration modes mainly constituted by phenol-ring vibrations, along with additional vibrations due to the amino acid backbone, should give rise to the vibronic bands. Normal mode analysis of stable conformer A under the OPLS-AA force field yields five normal modes (with frequencies 725, 781, 794, 834, and 852 cm^{-1}) in a frequency range that encompasses experimental and theoretical vibronic bands. Although the three lower frequencies are close to the frequency observed in the experimental spectrum, the normal modes associated with them turned out not to involve phenol-ring vibrations and should be irrelevant to the vibronic bands. The other two normal modes are constructed by a combination of two primary modes, the so-called "benzene breathing" mode and the torsional mode of the amino acid backbone. The two primary modes are in-phase in one normal mode and out-of-phase in the other.

The coupling strength of a vibrational mode to an electronic transition is usually described by a factor called the Huang−Rhys (HR) factor. This is proportional to the difference between the equilibrium positions of the mode in the excited electronic state and in the ground electronic state. From the simple relationship between the HR factor of the vibrational mode (S_{vib}) and the intensity of its vibronic band,[39] $S_{vib}^n/n! = I_n/I_0$ where I_n is the intensity of the nth band; the HR factor for the two normal modes is estimated to be about 0.77.

IV. Conclusion

Using photodissociation spectroscopy, we have studied the photodepletion spectrum of $TyrH^+$ in the gas phase at a moderately low temperature (150 K) in the excitation range from 34 800 through 37 500 cm^{-1}. Until recently, a few spectroscopic studies on protonated amino acids in the gas phase have been performed in a limited range of frequency, and they have focused on assignment of the fingerprint spectrum obtained at a cryogenic temperature to the origin bands of inhomogeneous conformers.[37,40] Meanwhile, in the present work, we have extended the spectral range wider to exhibit the spectral pattern including nonorigin bands.

Plausible conformations of molecular ions and their S0−S1 transition energies have been obtained, respectively, by density functional theory (B3LYP/6-311++G**) and ZINDO/S methods. With the assumption that the photodepletion yield should

be proportional to the probability of single-photon absorption, the photodepletion spectrum has been theoretically analyzed, for the first time, by the cumulant expansion method in conjunction with MD and ZINDO/S methods.

Absorption spectra of four stable molecular conformers have been calculated and compared with the photodepletion spectrum. The spectral pattern (appearance of multiple bands and their spectral widths) observed in the experiment has been reasonably reproduced by the theoretical method. Multiple spectral bands have been found to originate from the vibronic transitions associated with the two normal modes, which involve the "benzene breathing" vibration and the torsional motion of the amino acid backbone. Spectral broadening of each band has turned out to originate from thermal broadening of the low-frequency modes, which are strongly coupled to the electronic transition, of the stable conformers.

In a theoretical viewpoint, one might argue whether it is reasonable to employ the cumulant expansion method for the line shape calculation and the semiclassical approach for quantum time-correlation function.[16,17,34] At least for the present system, which has larger degrees of freedom than other small molecules often studied in the gas phase, we can confirm that both theoretical techniques are sufficiently accurate in calculation of the absorption spectrum (line shape function).

Acknowledgment. This work was supported by a research grant from Chungbuk National University in 2007.

References and Notes

(1) Rizzo, T. R.; Park, Y. D.; Levy, D. H. *J. Am. Chem. Soc.* **1985**, *107*, 277.

(2) Rizzo, T. R.; Park, Y. D.; Peteanu, L. A.; Levy, D. H. *J. Chem. Phys.* **1986**, *84*, 2534.

(3) Martinez, S. J., III; Alfano, J. C.; Levy, D. H. *J. Mol. Spectrosc.* **1992**, *156*, 421.

(4) Lindinger, A.; Toennies, J. P.; Vilesov, A. F. *J. Chem. Phys.* **1999**, *110*, 1429.

(5) Grace, L. I.; Cohen, R.; Dunn, T. M.; Lubman, D. M.; de Vries, M. S. *J. Mol. Spectrosc.* **2002**, *215*, 204.

(6) Zhang, M.; Huang, Z.; Lin, Z. *J. Chem. Phys.* **2005**, *122*, 134313.

(7) (a) Nolting, D.; Marian, C.; Weinkauf, R. *Phys. Chem. Chem. Phys.* **2004**, *6*, 2633. (b) Talbot, F. O.; Tabarin, T.; Antoine, R.; Broyer, M.; Dugourd, P. *J. Chem. Phys.* **2005**, *122*, 074310. (c) Dhzonson, A.; Maier, J. P. *Int. J. Mass Spectrom.* **2006**, *255*−*256*, 139.

(8) Kang, H.; Jouvet, C.; Dedonder-Lardeux, C.; Martrenchard, S.; Gregoire, G.; Desfrancois, C.; Schermann, J.-P.; Barat, M.; Fayeton, J. A. *Phys. Chem. Chem. Phys.* **2005**, *7*, 394.

(9) Boyarkin, O. V.; Mercier, S.; Kamariotis, A.; Rizzo, T. R. *J. Am. Chem. Soc.* **2006**, *128*, 2816.

(10) Sobolewski, A. L.; Domcke, W.; Dedonder-Lardeux, C.; Jouvet, C. *Phys. Chem. Chem. Phys.* **2002**, *4*, 1093.

(11) Gregoire, G.; Jouvet, C.; Dedonder, C.; Sobolewski, A. L. *J. Am. Chem. Soc.* **2007**, *129*, 6223.

(12) Cho, M. H.; Yu, J. Y.; Joo, T. H.; Nagasawa, Y.; Passino, S. A.; Fleming, G. R. *J. Phys. Chem.* **1996**, *100*, 11944.

(13) (a) Joo, T. H.; Jia, Y. W.; Yu, J. Y.; Lang, M. J.; Fleming, G. R. *J. Chem. Phys.* **1996**, *104*, 6089. (b) de Boeij, W. P.; Pshenichnikov, M. S.; Wiersma, D. A. *J. Phys. Chem.* **1996**, *100*, 11806.

(14) (a) Piryatinski, A.; Lawrence, C. P.; Skinner, J. L. *J. Chem. Phys.* **2003**, *118*, 9664. (b) Piryatinski, A.; Lawrence, C. P.; Skinner, J. L. *J. Chem. Phys.* **2003**, *118*, 9672.

(15) (a) Marchi, M.; Gehlen, J. N.; Chandler, D.; Newton, M. *J. Am. Chem. Soc.* **1993**, *115*, 4178. (b) Kwac, K.; Lee, C.; Jung, Y.; Han, J.; Kwak, K.; Zheng, J.; Fayer, M. D.; Cho, M. *J. Chem. Phys.* **2006**, *125*, 244508. (c) Corcelli, S. A.; Lawrence, C. P.; Skinner, J. L. *J. Chem. Phys.* **2004**, *120*, 8107.

(16) Kwac, K.; Cho, M. *J. Chem. Phys.* **2003**, *119*, 2247.

(17) Gorbunov, R. D.; Nguyen, P. H.; Kobus, M.; Stock, G. *J. Chem. Phys.* **2007**, *126*, 054509.

(18) Chelli, R.; Volkov, V. V.; Righini, R. J. *Comput. Chem.* **2008**, *29*, 1507.

(19) Yoon, T. O.; Choi, C. M.; Kim, H. J.; Kim, N. J. *Bull. Korean Chem. Soc.* **2007**, *28*, 619.

(20) Wang, X.-B.; Yang, J.; Wang, L.-S. *J. Phys. Chem. A* **2008**, *112*, 172.

(21) Guan, S.; Marshall, A. G. *Int. J. Mass Spectrom.* **1996**, *157/158*, 5.

(22) Doroshenko, V. M.; Cotter, R. J. *Rapid Commun. Mass Sp.* **1996**, *10*, 65.

(23) (a) Gilb, S.; Jacobsen, K.; Schooss, D.; Furche, F.; Ahlrichs, R.; Kappes, M. M. *J. Chem. Phys.* **2004**, *121*, 4619. (b) Nonose, S.; Taguchi, T.; Chen, F.; Iwata, S.; Fuke, K. *J. Phys. Chem. A* **2002**, *106*, 5242. (c) Takasu, R.; Nishikawa, K.; Miura, N.; Sabu, A.; Hashimoto, K.; Schulz, C. P.; Hertel, I. V.; Fuke, K. *J. Phys. Chem. A* **2001**, *105*, 6602.

(24) Lindahl, E.; Hess, B.; van der Spoel, D. *J. Mol. Model.* **2001**, *7*, 306.

(25) Kaminski, G. A.; Friesner, R. A.; Tirado-Rives, J.; Jorgensen, W. L. *J. Phys. Chem. B* **2001**, *105*, 6474.

(26) Zerner, M. *Rev. Comput. Chem.* **1991**, *2*, 313.

(27) Frisch, M. J.; Trucks, G. W.; Schlegel, H. B.; Scuseria, G. E.; Robb, M. A.; Cheeseman, J. R.; Montgomery, J. A., Jr.; Vreven, T.; Kudin, K. N.; Burant, J. C.; Millam, J. M.; Iyengar, S. S.; Tomasi, J.; Barone, V.; Mennucci, B.; Cossi, M.; Scalmani, G.; Rega, N.; Petersson, G. A.; Nakatsuji, H.; Hada, M.; Ehara, M.; Toyota, K.; Fukuda, R.; Hasegawa, J.; Ishida, M.; Nakajima, T.; Honda, Y.; Kitao, O.; Nakai, H.; Klene, M.; Li, X.; Knox, J. E.; Hratchian, H. P.; Cross, J. B.; Bakken, V.; Adamo, C.; Jaramillo, J.; Gomperts, R.; Stratmann, R. E.; Yazyev, O.; Austin, A. J.; Cammi, R.; Pomelli, C.; Ochterski, J. W.; Ayala, P. Y.; Morokuma, K.; Voth, G. A.; Salvador, P.; Dannenberg, J. J.; Zakrzewski, V. G.; Dapprich, S.; Daniels, A. D.; Strain, M. C.; Farkas, O.; Malick, D. K.; Rabuck, A. D.; Raghavachari, K.; Foresman, J. B.; Ortiz, J. V.; Cui, Q.; Baboul, A. G.; Clifford, S.; Cioslowski, J.; Stefanov, B. B.; Liu, G.; Liashenko, A.; Piskorz, P.; Komaromi, I.; Martin, R. L.; Fox, D. J.; Keith, T.; Al-Laham, M. A.; Peng, C. Y.; Nanayakkara, C. G.; Challacombe, M.; Gill, P. M. W.; Johnson, B. G.; Chen, W.; Wong, M. W.; Gonzalez, C.; Pople, J. A. *Gaussian 03, Revision D.01*; Gaussian, Inc.: Pittsburgh, PA, 2003.

(28) McQuarrie, D. A. *Statistical Mechanics*; University Science Books: Sausalito, CA, 2000.

(29) Mukamel, S. *Principles of Nonlinear Optical Spectroscopy*, 2nd ed.; Oxford University Press: New York, 1995.

(30) Berne, B. J.; Harp, G. D. *Adv. Chem. Phys.* **1970**, *17*, 63.

(31) Oxtoby, D. W. *Adv. Chem. Phys.* **1981**, *47*, 487.

(32) Bader, J. S.; Berne, B. J. *J. Chem. Phys.* **1994**, *100*, 8359.

(33) (a) Egorov, S. A.; Everitt, K. F.; Skinner, J. L. *J. Phys. Chem. A* **1999**, *103*, 9494. (b) Kim, H.; Rossky, P. J. *J. Phys. Chem. B* **2002**, *106*, 8240.

(34) Lawrence, C. P.; Skinner, J. L. *Proc. Natl. Acad. Sci. U.S.A.* **2005**, *102*, 6720.

(35) (a) Berens, P. H.; White, S. R.; Wilson, K. R. *J. Chem. Phys.* **1981**, *75*, 515. (b) Frommhold, L. *Collision-induced absorption in gases*; Cambridge University Press: Cambridge, U.K., 1993; Vol. 2.

(36) Berendsen, H. J. C.; Postma, J. P. M.; van Gunsteren, W. F.; DiNola, A.; Haak, J. R. *J. Chem. Phys.* **1984**, *81*, 3684.

(37) Stearns, J. A.; Mercier, S.; Seaiby, C.; Guidi, M.; Boyarkin, O. V.; Rizzo, R. C. *J. Am. Chem. Soc.* **2007**, *129*, 11814.

(38) Schmidt, J. R.; Corcelli, S. A.; Skinner, J. L. *J. Chem. Phys.* **2005**, *123*, 044513.

(39) Yang, M. *J. Mol. Spectrosc.* **2006**, *239*, 108.

(40) Mercier, S. R.; Boyarkin, O. V.; Kamariotis, A.; Guglielmi, M.; Tavernelli, I.; Cascella, M.; Rothlisberger, U.; Rizzo, T. R. *J. Am. Chem. Soc.* **2006**, *128*, 16938.

JP809573A